



Published in final edited form as:

Mol Cell. 2018 November 15; 72(4): 778–785.e3. doi:10.1016/j.molcel.2018.09.008.

MICU1 interacts with the D-ring of the MCU pore to control its Ca²⁺ flux and sensitivity to Ru360

Melanie Paillard¹, György Csordás¹, Kai-Ting Huang¹, Peter Várnai², Suresh K. Joseph¹, and György Hajnóczky^{1,3,*}

¹MitoCare Center, Department of Pathology, Anatomy and Cell Biology, Thomas Jefferson University, Philadelphia, PA 19107, USA

²Department of Physiology, Semmelweis University, Budapest, Hungary

³Lead Contact

SUMMARY

Proper control of the mitochondrial Ca²⁺ uniporter's pore (MCU) is required to allow Ca²⁺ dependent activation of oxidative metabolism and to avoid mitochondrial Ca²⁺ overload and cell death. The MCU's gatekeeping and cooperative activation is mediated by the Ca²⁺ sensing MICU1 protein, which has been proposed to form dimeric complexes anchored to the EMRE scaffold of MCU. We unexpectedly find that MICU1 suppresses inhibition of MCU by ruthenium red/Ru360, which bind to MCU's DIME motif, the selectivity filter. This led us to recognize in MICU1's sequence, a putative DIME Interacting Domain (DID) which is required for both gatekeeping and cooperative activation of MCU and for cell survival. Thus, we propose that MICU1 has to interact with the D-ring formed by the DIME domains in MCU to control the uniporter.

Graphical Abstract

*Correspondence: Dr. György Hajnóczky, MitoCare Center, Department of Pathology, Anatomy and Cell Biology, Suite 527 JAH, Thomas Jefferson University, Philadelphia PA 19107, USA, Tel. (215) 503-1427, Fax. (215) 923-2218, gyorgy.hajnoczky@jefferson.edu.

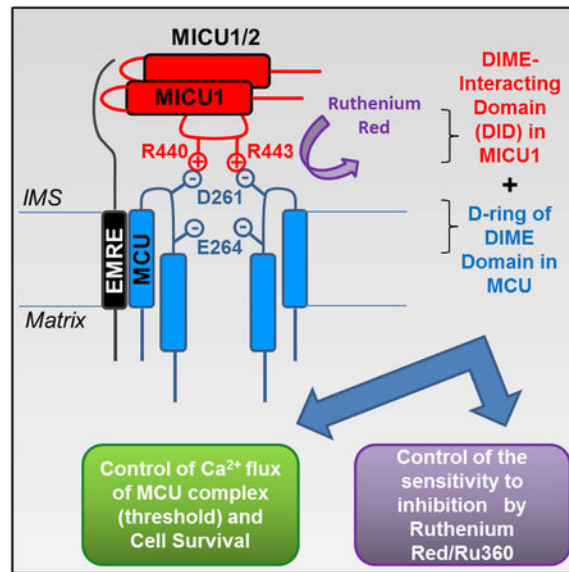
AUTHORS CONTRIBUTION

Conceptualization: G.H., G.C., S.K.J. and M.P.; Investigation: G.H., G.C., S.K.J., M.P., K.T.H. and P.V.; Writing: G.H., G.C., S.K.J. and M.P.; Funding Acquisition: G.H., M.P.

DECLARATION OF INTERESTS

The authors declare no competing interests.

Publisher's Disclaimer: This is a PDF file of an unedited manuscript that has been accepted for publication. As a service to our customers we are providing this early version of the manuscript. The manuscript will undergo copyediting, typesetting, and review of the resulting proof before it is published in its final citable form. Please note that during the production process errors may be discovered which could affect the content, and all legal disclaimers that apply to the journal pertain.



eTOC blurb

Paillard et al. report that mitochondrial Ca²⁺ uptake 1 (MICU1) interacts with the D-ring of MCU, the pore forming protein of the mitochondrial Ca²⁺ uniporter, through a DIME-interacting domain involving the arginines 440 and 443, to control both the Ca²⁺ flux and the Ruthenium Red sensitivity of the MCU complex.

Keywords

mitochondria; Ca²⁺ uptake; threshold; cooperativity; calcium signaling; oxidative stress

INTRODUCTION

The mitochondrial Ca²⁺ uniporter (mtCU) or MCU complex needs to be tightly regulated to avoid cell death by Ca²⁺ overload and to allow the Ca²⁺ dependent physiological stimulation of oxidative metabolism. Among the different components of the MCU complex, the Ca²⁺-sensing protein MICU1 has been characterized as a key mediator of gatekeeping and cooperative activation of MCU, the pore-forming unit of the MCU complex (Csordas et al., 2013; Kamer and Mootha, 2014; Mallilankaraman et al., 2012; Patron et al., 2014). MICU1 has been linked to human neurological and muscular diseases (Lewis-Smith et al., 2016; Logan et al., 2014), as well as to liver regeneration (Antony et al., 2016), cardiac ischemia-reperfusion injury (Xue et al., 2017), diabetic cardiomyopathy (Ji et al., 2017) and ovarian cancer (Chakraborty et al., 2017).

In addition to MCU and MICU1, other MCU complex components have also been identified: two paralogs of MICU1, MICU2 and MICU3 (Plovanich et al., 2013), a dominant negative paralog of MCU, MCUB (Raffaello et al., 2013), and the indispensable transmembrane protein EMRE (Sancak et al., 2013). MICU1 interacts with MICU2 through a disulfide bond involving C465 in MICU1 and C410 in MICU2, to form homo/

heterodimers which control the MCU complex activity (Patron et al., 2014; Petrunaro et al., 2015). On the other hand, MICU1 binding to the polyaspartate tail of EMRE has been shown to anchor MICU1 to the MCU complex in the mitochondrial intermembrane space and thus confer gatekeeping of the pore (Tsai et al., 2016). However, in the same study, MICU1's interaction with MCU without EMRE was also shown by coimmunoprecipitation (Tsai et al., 2016), which is also supported by surface plasmon resonance data (Vecellio Reane et al., 2016).

Topology studies showed that most of MCU's amino acid residues are in the two transmembrane domains and the N- and C-termini that are exposed to the mitochondrial matrix, and identified a short sequence between the two transmembrane domains, which is exposed to the intermembrane space (IMS) and might be accessible for direct interaction with IMS proteins like MICU1. This motif was termed as DIME (or DXXE) based on its amino acid sequence conserved across species (D261 and E264 in hSMCU) (Baughman et al., 2011). A recent study characterized the DIME domain as the ion selectivity filter of the MCU with ion binding to the two carboxylate rings (Cao et al., 2017). Notably, mutation of DIME domain also impaired the MICU1-MCU interaction (Patron et al., 2014). Interestingly, the inhibitory effect of the most potent inhibitors of the MCU complex, ruthenium red (RuRed) and ruthenium 360 (Ru360), requires S259 (Baughman et al., 2011). Two recent NMR studies further indicated that Ru360/RuRed binds the D-ring of MCU's selectivity filter, which is solvent-exposed compared to the E-ring located deeper in the pore (Arduino et al., 2017; Cao et al., 2017). Thus, we reasoned that MICU1 might affect the RuRed sensitivity of the MCU complex through a potential interaction with the DIME domain of MCU.

We here, find that MICU1 deletion increases the MCU complex sensitivity to RuRed/Ru360, suggesting that MICU1 interferes with the binding site of these inhibitors in the DIME motif of MCU. We then identify a complementing sequence in MICU1 to the DIME motif, which we refer to as DIME interacting domain (DID) and predict that two arginines (R440 and R443) engage in potential salt bridges with the D-ring of MCU. Using an imaging approach to assess both threshold and cooperativity of the MCU complex in MICU1-KO mouse embryonic fibroblasts (MEFs) and HEK293 cells (HEKs), we show that the DID in MICU1 is required to control the MCU complex-mediated Ca^{2+} influx and in turn, cell survival. Finally, we show that the DID of MICU1 alters the RuRed/Ru360 sensitivity by competing for the interaction with the DIME domain of MCU, thus opening a new avenue for therapeutic targeting of the MCU complex.

RESULTS

MICU1 controls the RuRed/Ru360 sensitivity of the MCU complex

While recording mitochondrial clearance of Ca^{2+} added to the cytoplasmic buffer of permeabilized hepatocytes isolated from wild type (Ctrl) and hepatocyte-specific MICU1^{-/-} mouse (MICU1-KD), we noticed that deletion of MICU1 caused sensitization to RuRed, (Figures 1A and 1B). Specifically, MICU1-deficient mitochondria showed less effective uptake when a large Ca^{2+} bolus was applied (50 μM CaCl_2) as we reported earlier (Antony et al., 2016) and it was almost completely suppressed by a submaximal dose of RuRed

(100nM), which caused only a small inhibition in wild type (WT) mitochondria. When dose response curves were compiled, almost an order of magnitude increase in sensitivity for RuRed was observed in MICU1-deficient hepatocytes (Figure 1C). Higher sensitivity to RuRed was also observed in MICU1-deficient hepatocytes in response to a smaller bolus of Ca^{2+} (7 μM ; raising $[\text{Ca}^{2+}]_c$ to 1.5-2 μM) (Figure S1), for which the mitochondrial Ca^{2+} uptake is similar to the control (Antony et al., 2016). The sensitivity was also increased towards Ru360 that is a more specific inhibitor of MCU complex (Figure 1D). Furthermore, sensitization to RuRed by MICU1 deletion was also found in MEFs (Figure 1E) and in HEKs (Figure 1F). Thus, these results provide evidence that MICU1 decreases the RuRed/Ru360 sensitivity of the MCU complex, probably by competing with RuRed/Ru360 for binding to MCU.

MICU1 has a complementing sequence to the region of MCU determining RuRed sensitivity and Ca^{2+} selectivity

RuRed/Ru360 was recently shown to bind the DIME domain of MCU (Arduino et al., 2017; Baughman et al., 2011; Cao et al., 2017). The results shown in Figure 1 led us to postulate that there might be a domain in MICU1 which interacts with the DIME domain of MCU. It has been previously suggested that MICU1 interacts indirectly with MCU through EMRE, involving the transmembrane domains of MCU and EMRE, and EMRE binding to MICU1 via EMRE's C-terminal polyaspartate tail (Sancak et al., 2013; Tsai et al., 2016). Nevertheless, two studies using different techniques have indicated that MICU1 can interact with MCU without EMRE (Tsai et al., 2016; Vecellio Reane et al., 2016), supporting the possibility of an additional protein-protein interaction component. Moreover, along with the DIME domain of MCU (Patron et al., 2014), the C-terminal structure of MICU1 has been shown to be necessary for co-immunoprecipitation with MCU (Kamer and Mootha, 2014; Wang et al., 2014). However, the exact sequence in MICU1 involved in the binding to MCU is still unknown. Alignment of MICU1, 2 and 3 revealed a potential DIME interacting domain in the C-terminal sequence of all three MICUs, involving lysine K438 and two arginines R440 and R443 which could form potential salt bridges with the DIME domain in MCU (Figure 2A). Among the marked potential interactions, the one between K438 and the corresponding serine is more likely a dipole-dipole interaction than actual salt bridge between the positively charged amino group of lysine and the OH of serine. The crystal structure of MICU1 shows that the two arginine residues are orientated in the same direction in a helix (Wang et al., 2014), thus suggesting that the side-chains of R440 and R443 could act like RuRed to bind to the outer D-ring of the pore of the MCU pentamer (Cao et al., 2017). To validate our hypothesis, we mutated in hsMICU1 these 3 residues to alanine (MICU1- DID: 440KQRLMR445>440AQALMA445) and analyzed its binding with MCU. MICU1- DID (tagged with HA) was pulled-down 60% less than WT MICU1 by MCU (tagged with FLAG) and, MCU was pulled-down in a lesser extent by MICU1- DID than WT MICU1 (Figure 2B). These results suggest that the KQRLMR sequence in MICU1, which we now named as DID (DIME Interaction Domain), interacts with MCU, probably through its DIME motif.

Next, using MICU1-KO MEFs, in which MICU2 is maintained (Antony et al., 2016), we aimed at better characterizing the functional role of the DID in MICU1 in the control of the

MCU complex Ca^{2+} flux. To assess MCU complex activity in individual cells, $[\text{Ca}^{2+}]_m$ was followed via loading the mitochondria in WT and MICU1-KO MEF cells with the ratiometric probe furaFF/AM; cells were then permeabilized and subjected to a 2-step Ca^{2+} addition protocol (3 and 20 μM CaCl_2 , 3 and 20Ca). Mitochondrial localization of the probe was confirmed by complete inhibition of the Ca^{2+} response by RuRed (Figure S2) (Paillard et al., 2017). As expected, MICU1-KO MEFs displayed an increased resting $[\text{Ca}^{2+}]_m$, which could be prevented by RuRed (Figure S2). The resting $[\text{Ca}^{2+}]_m$ was used then as a measure of gatekeeping activity of various MICU1 mutants. Rescue was performed with wild type MICU1 (MICU1-HA) or MICU1- DID in the MICU1-KO cells. While MICU1-HA restored the low resting $[\text{Ca}^{2+}]_m$, MICU1- DID failed to lower it (Figure 2C,D). As a simple measure of the Ca^{2+} -induced highly cooperative activation of MCU, in a single-addition protocol, the initial response to 20Ca (difference between the $[\text{Ca}^{2+}]_m$ 30s post-20Ca addition and the resting $[\text{Ca}^{2+}]_m$) was used. MICU1- DID expression decreased $[\text{Ca}^{2+}]_m$ as in MICU1-KO MEFs (with empty vector), compared to WT MEFs (Figures 2C,E). Thus, our data supports that mutation of the complementing sequence with MCU DIME motif interferes with MICU1 binding to and control of the Ca^{2+} fluxes of MCU.

Role of DID and the other motifs of MICU1 in intracellular Ca^{2+} homeostasis and cell survival

MICU1 is thus engaged in at least 3 interactions with components of the MCU complex: the previously documented dimerization with MICU2/MICU1, an interaction with EMRE, and our newly demonstrated interaction with MCU via the DID. To evaluate the MCU complex regulation by the interactions of MICU1 with MICU2, EMRE and MCU respectively, we interfered with each separately or in combination and performed simultaneous $[\text{Ca}^{2+}]_c$ and $[\text{Ca}^{2+}]_m$ measurements during store-operated Ca^{2+} entry (SOCE) in intact WT and MICU1-KO HEKs. We opted for SOCE as the Ca^{2+} source because it stimulates mitochondrial Ca^{2+} uptake mostly via the global $[\text{Ca}^{2+}]_c$ increase that we measured, so we could plot $[\text{Ca}^{2+}]_m$ both as a function of time and $[\text{Ca}^{2+}]_c$. We generated three additional HA-tagged mutants of MICU1: the MICU1- dimer (C465A), which is incompetent for dimerization, MICU1- EMRE (99KKKKR>99AAAAA) that lacks the EMRE-binding motif and a combination of MICU1- DID+ EMRE+ dimer. Co-transfection of MICU1-KO cells with MICU1 mutants and the mitochondrial matrix targeted Ca^{2+} indicator, mtCepia, allowed us to evaluate in each single cell $[\text{Ca}^{2+}]_m$ and $[\text{Ca}^{2+}]_c$ by fura2 (Figures 3A-B). The SOCE-mediated $[\text{Ca}^{2+}]_m$ increase appeared earlier in MICU1-KO HEK cells rescued by either the empty vector, the MICU1- DID or the MICU1- DID+ EMRE+ dimer mutant, compared to WT HEKs or MICU1-KO cells rescued by the other MICU1 mutants (Figure 3B). The $[\text{Ca}^{2+}]_m$ response 60s post- Ca^{2+} addition revealed that both MICU1- DID and MICU1- DID+ EMRE + dimer mutant rescued took up Ca^{2+} similarly to the MICU1-KO cells while the MICU1- EMRE and MICU1- dimer rescued cells took up initially less Ca^{2+} like the WT MICU1 rescue (Figure 3C). Plotting $[\text{Ca}^{2+}]_m$ against $[\text{Ca}^{2+}]_c$ further supported that MICU1-KO cells rescued either by the empty vector or the MICU1- DID or the MICU1- DID+ EMRE + dimer mutant, showed a significant $[\text{Ca}^{2+}]_m$ increase at lower $[\text{Ca}^{2+}]_c$ than WT cells or the ones rescued by WT MICU1 and the other MICU1 mutants in MICU1-KO HEKs (Figure 3D). Indeed, to reach a similar level of $[\text{Ca}^{2+}]_m$ (arbitrarily set at 1.2 ratio units), around 0.2 μM of $[\text{Ca}^{2+}]_c$ was sufficient in MICU1-KO and the MICU1- DID or MICU1-

DID+ EMRE+ dimer rescues, whereas WT HEKs and MICU1-KO cells rescued by WT MICU1, MICU1- EMRE or MICU1- dimer constructs required a significantly higher $[Ca^{2+}]_c$ (Figure 3E). We further assessed if the MICU1- DID mutant operated as a dominant-negative MCU complex component in these intact cells experiments. Similarly to MICU1-KO HEKs, co-expression of WT MICU1 and MICU1- DID led to a significant $[Ca^{2+}]_m$ increase at lower $[Ca^{2+}]_c$ than MICU1-KO HEKs rescued by WT MICU1 itself or along with a point mutant in EF1 of MICU1 (MICU1-EF1-D9E), thus unraveling a dominant-negative effect of MICU1- DID over WT MICU1 (Figures S3A-B). MICU1-EF1-D9E was created to cause a specific perturbation in D239 of the EF hand but it was found to unalter the resting $[Ca^{2+}]_m$ or the rescue of cooperativity and Ca^{2+} dependent activation of MCU complex (Figures S3C-E). Therefore, we used this construct as an alternative example of full rescue. Together, these data suggest that the MICU1-MCU interaction through the MICU1's DID and MCU's DIME motif is the most critical for the gatekeeping of the MCU complex.

Because the gatekeeping of MCU complex by MICU1 is central to avoiding mitochondrial Ca^{2+} overload, oxidative stress and cell death (Antony et al., 2016; Csordas et al., 2013; Liu et al., 2016; Mallilankaraman et al., 2012), we then proceeded to study the so-called delayed Ca^{2+} dysregulation by following the $[Ca^{2+}]_c$ in intact HEKs subjected to prolonged Ca^{2+} entry (Figure 3F). After the initial $[Ca^{2+}]_c$ rise a large delayed increase was observed only in mock- and MICU1- DID-rescued cells, whereas $[Ca^{2+}]_c$ was maintained at a low level in MICU1-KO HEKs rescued by WT MICU1 or with the MICU1-EF1-D9E (Figure 3G).

The mitochondrial oxidative stress generated during prolonged SOCE conditions was measured using mtGrx1-RoGFP2, the fluorescence of which shows the ratio of oxidized and reduced glutathione (GSSG/GSH) and is unaffected by pH (Gutscher et al., 2008). The oxidative stress recorded in mock rescued cells was duplicated in the cells rescued by the MICU1- DID mutant, whereas oxidative stress was avoided in the cells rescued with WT MICU1 or MICU1-EF1-D9E constructs (Figure 3H). Importantly, all the MICU1 constructs were effectively expressed in the MICU1-KO cells, with no difference between the MICU1- DID and MICU1-EF1-D9E mutants (Figure S4A). To conclude, these results indicate that MICU1 interaction with the D-ring of the DIME domain of MCU is required for gatekeeping of the MCU complex and in turn for cell survival.

DID mutant fails to rescue RuRed sensitivity

Finally, we investigated how RuRed sensitivity will be altered with expression of DID mutant of MICU1. While in WT and in MICU1-KO HEKs rescued by WT MICU1, or MICU1-EF1-D9E constructs, 30nM RuRed elicited a partial inhibition of the mitochondrial Ca^{2+} uptake rate, MICU1-KO HEKs rescued with empty vector or MICU1- DID displayed an almost complete inhibition of mitochondrial Ca^{2+} uptake, which could be only attained with 3 μ M RuRed in WT HEKs (Figure 4A-B). Indeed, a significantly higher inhibition of mitochondrial Ca^{2+} uptake by 30nM RuRed was obtained in MICU1-KO HEKs rescued with empty vector or MICU1- DID compared to either WT MICU1 or MICU1-EF1-D9E rescue (Figure 4B). Importantly, rescuing MICU1-KO HEKs by the MICU1- DID or MICU1-EF1-D9E constructs both lead to a higher MICU1 protein expression than that in

the WT HEK cells (Figure S4B). Because no release of any of the MICU1 constructs was noticed upon selective permeabilization of the plasma membrane and in the immunofluorescence experiments the expressed MICU1 constructs co-localized with the mitochondria (Figure S4C), they seem to be correctly targeted to the mitochondria. To test the localization to the IMS and proper interaction with EMRE for both MICU1-HA and MICU1- DID-HA, we performed for the revision an immunoprecipitation experiment. Figure S4D shows that EMRE (tagged with Myc) pulled-down a comparable amount of WT MICU1 and MICU1- DID mutant (tagged with HA), thus confirming the proper localization of the MICU1- DID construct in the IMS and also that alteration of the MICU1-MCU interaction does not interfere with the MICU1-EMRE binding. Furthermore, the dominant negative effect of MICU1- DID (Figure S3AB), also provides a functional evidence for the correct localization of MICU1- DID. Thus, the failure of the DID mutant to restore the lower RuRed sensitivity confirms that the interaction between the DID of MICU1 and MCU, likely through its DIME domain, controls the Ca^{2+} flux and the RuRed sensitivity of the MCU complex.

DISCUSSION

The main finding of this study is that MICU1 interacts with the DIME motif of MCU and this interaction is required for both keeping MCU complex's pore closed at low $[\text{Ca}^{2+}]_c$ and optimally activated at high $[\text{Ca}^{2+}]_c$. Furthermore, this interaction also controls the MCU complex's accessibility for its most characterized inhibitors. Thus, our findings are central to understanding the mechanisms that allow MICU1 to support cell survival by preventing mitochondrial Ca^{2+} overload and cause human disease in MICU1 deficiency, and provide important clues for mitochondrial drug development.

It has been broadly recognized that the Ca^{2+} -sensing MICU1 is required for the control of MCU complex activity. As to the underlying mechanism, MICU1's interactions with some components of the MCU complex have been dissected recently: disulfide bonds between the cysteines of MICU1 and MICU2 to form dimers (Patron et al., 2014; Petrunaro et al., 2015) and electrostatic interaction between the polyaspartate tail of EMRE and the polybasic sequence of MICU1 (Tsai et al., 2016). While Hoffman et al. had suggested a potential interaction between the N-terminal polybasic domain of MICU1 and the two interacting coiled-coil domains of MCU (Hoffman et al., 2013), this was later demonstrated to be indirect and mediated through EMRE (Tsai et al., 2016). MICU1's interaction with MCU without EMRE was also indicated (Kovacs-Bogdan et al., 2014; Tsai et al., 2016) but until now, no direct interaction sites between MCU and MICU1 have been established. Given the involvement of the MCU complex and specifically, MICU1 in cell death and in diseases (Liu et al., 2017; Mammucari et al., 2017), a better understanding of the MICU1 interactions in the MCU complex was clearly needed.

We here reported a structural and functional interaction between the DID of MICU1 and the region identified as the selectivity filter domain of MCU, which controls the Ca^{2+} flux and the RuRed sensitivity of the MCU complex. Using sequence alignment, we identified a putative DIME interacting domain, DID, in the C-terminus of MICU1, engaging R440 and R443 in potential salt bridges with the D-ring of MCU. Decreased co-immunoprecipitation

between MCU and a MICU1 mutant of these two arginines (MICU1- DID: 440KQRLMR445>440AQALMA445) supported a structural role for the DID in MICU1-MCU interaction. Using Ca²⁺ imaging approaches in genetically rescued MICU1-KO MEFs and HEKs cells, we showed that the DID in MICU1 is required for both the threshold and cooperative activation of the MCU complex-mediated Ca²⁺ uptake. Furthermore, the DID was required to avoid mitochondrial Ca²⁺ overload, ROS dysregulation and the ensuing cell injury. Additionally, unlike MICU1, MICU1- DID expression in MICU1-KO HEKs did not decrease the RuRed sensitivity. Based on the proposed *in vitro* architecture of MCU as a pentamer (Oxenoid et al., 2016) and on our identification of the MICU1 DID interaction site with MCU, we here propose an updated model of the interactions of MICU1 within the MCU complex (Figure 4C): the two arginines R440 and R443 from one MICU1 would interact with the exposed D-ring (D261) of two MCU units from the pentamer to assure the physiological gatekeeping of the pore. In such a model, however it would be predicted that only one MICU1 dimer is required to block a pentameric MCU complex. Nevertheless, the pentameric assembly was established *in vitro* using *C. elegans* MCU that lacked the N-terminal 165 amino acids (Oxenoid et al., 2016) and the *in vivo* MCU stoichiometry is yet to be determined. Some earlier studies, based on biochemical data, proposed tetrameric stoichiometry (Raffaello et al., 2013), in which case our model would be compatible with a pair of DID domains (in 2 MICU1 dimers) being able to fully engage with the D-ring of the MCU selectivity filter. Thus, elucidation of the *in vivo* architecture of MCU will be crucial to better appreciate the stoichiometry between MICU1 and MCU per MCU complex.

As to the relevance of the interactions with the different MCU complex components, our results identify the MICU1 interaction with MCU via its DID to be critical for the gatekeeping. In our experiments, relevance of EMRE and dimer formation is also confirmed but the MICU1-EMRE interaction rather appears as an additional stabilizing interaction to support the tight regulation of MCU by MICU1, which also fits with the only partial loss of threshold observed by Tsai et al. when disrupting the MICU1-EMRE interaction (Tsai et al., 2016). Notably, direct control of MCU by MICU1 as an evolutionary conserved critical factor in gatekeeping is supported by the finding that the functional MCU complex of *Dictyostelium discoideum* consists of only MCU and one MICU isoform (Kovacs-Bogdan et al., 2014).

Our alignment of MICUs suggests that the DID, comprising of the two arginines, is conserved among the three MICUs. However, MICU2 fails to act as a gatekeeper in the absence of MICU1 (Kamer and Mootha, 2014). Because some interactions remained between MICU1- DID and MCU (Figure 2B) we speculate those interactions might be different for MICU1 and MICU2. Thus, further studies will be required to test whether the DID of MICU2 (or MICU3) can support an interaction with MCU.

One of the most unexpected finding of this work was that removal of MICU1 greatly sensitized mitochondria towards RuRed/Ru360 and this seems to be because of the DID limiting access of RuRed to its target site in the DIME of MCU. In the light of recent demonstration of tissue-specific differences in the MICU1 abundance relative to MCU (Paillard et al., 2017), the present finding might predict different RuRed/Ru360 sensitivity of MCU complex in various tissues, such as the particularly high sensitivity in the little

MICU1-containing cardiac muscle (Matlib et al., 1998). Furthermore, pharmacological targeting of the MCU complex by new and potentially therapeutically useful molecules has become an area of concerted research efforts (Arduino et al., 2017; D and Perocchi, 2018). Our findings might aid drug design and call attention to possible organ-specific differences in the sensitivity to future drugs sharing the target of RuRed/Ru360.

STAR METHODS

CONTACT FOR REAGENT AND RESOURCE SHARING

Further information and requests for resources and reagents should be directed to and will be fulfilled by the Lead Contact, Gyorgy Hajnoczky (gyorgy.hajnoczky@jefferson.edu).

EXPERIMENTAL MODEL AND DETAILS

Cell lines—Mouse embryonic fibroblasts (MEFs) were isolated by trypsin digestion from e14.5 embryos, using *MICU1^{KO/loxP}* mice (for generation see (Antony et al., 2016)), and then immortalized. MEFs were cultured in DMEM (ATCC 30-2002) supplemented with penicillin, streptomycin at 37°C/5% O₂. MICU1-KO, and EMRE-KO HEK cells were kindly provided by Dr Vamsi Mootha and grown as previously described (Sancak et al., 2013) and the stable MCU-Flag HEK by Dr Shey-Shing Sheu. Co-transfection of the control plasmid (pcDNA3-dest40) or the HA-tagged MICU1 constructs with the mitochondrial Ca²⁺ sensor mtCepia or the redox sensor mtGrx1-RoGFP2, was performed in MEFs and HEKs using Lipofectamine 3000 according to manufacturers' protocol. Co-transfection efficiency was confirmed by immunofluorescence via the HA tag (data not shown). Since a 4-fold higher expression was observed for the WT MICU1-HA construct compared to the other MICU1-HA mutants, we used ¼ of the DNA amount for the WT MICU1-HA plasmid.

Primary mouse hepatocytes—Primary hepatocytes were isolated by in situ retrograde perfusion with collagenase as previously described (Csordas et al., 2013), from *MICU1^{loxP/loxP}* male mice 3 weeks after tail vein-injection with an AAV8-TBG-Cre or an AAV8-TBG-Null (1.3×10¹¹ pfu/mouse) (Penn Vector Core). Only preparations with greater than 90% viability were used for subsequent experiments.

METHOD DETAILS

Measurements of mitochondrial Ca²⁺ uptake and membrane potential—Saponin-permeabilized hepatocytes (2 millions), MEFs or HEKs (2.4 mg) were resuspended in 1.5 mL of intracellular medium (ICM) containing 120 mM KCl, 10 mM NaCl, 1 mM KH₂PO₄, 20 mM Tris-HEPES at pH 7.2, and supplemented with proteases inhibitors (leupeptin, antipain, pepstatin, 1mg/ml each), 2 mM MgATP, 2 μM thapsigargin and maintained in a stirred thermostated cuvette at 35°C. Assays were performed in presence of 20 μM CGP-37157 and 1 mM succinate using a multiwavelength-excitation dual-wavelength-emission fluorimeter (DeltaRAM, PTI). The extramitochondrial Ca²⁺ concentration [Ca²⁺]_c was assessed using the ratiometric Ca²⁺ probe Fura2-FA (1.5 μM, Teflabs) or Fura-loAff (formerly Fura-FF) (1 μM, Teflabs). ψ_m was measured with 1.5 μM TMRM (Invitrogen). Fura and TMRM fluorescence were recorded simultaneously using 340-380 nm excitation and 500 nm emission, and 545 nm excitation and 580 nm emission,

respectively. Complete depolarization (maximum de-quench of TMRM fluorescence) was elicited using of the protonophore FCCP (2 μ M). Calibration of the Fura signal was carried out at the end of each measurement, adding 1 mM CaCl₂, followed by 10 mM EGTA/Tris, pH 8.5.

Construction of the HA-tagged MICU1 mutants—MICU1-EF1-D9E and MICU1-EMRE were generated by site-directed mutagenesis in the cDNA sequence pcDNA-DEST40 containing the wild type human MICU1 (provided by Vamsi K. Mootha). MICU1-DID was created by inserting the synthesized sequence coding the appropriate mutations (Blue Heron) between the HindII/EcoNI restriction sites. Finally, the sequence resulting the C-terminal HA tag was inserted into each construct between the EcoNI/AgeI restriction sites. All constructs have been sequenced.

Co-immunoprecipitation—For co-IP experiments, HEK293 cells were grown in 10cm plates. After 48h post-transfection the plates were lysed in 1ml of a buffer containing 120mM NaCl, 50mM MOPS (pH 7.2), 0.5mM EGTA, 1% 3-[(3-Cholamidopropyl)dimethylammonio]-1-propanesulfonate hydrate (CHAPS) and protease inhibitor cocktail. Two equal aliquots (approximately 0.5mg protein) were immunoprecipitated with either 15 μ l FLAG-Ab beads or 1 μ g of HA or Myc antibody with 50 μ l of Protein A sepharose (50% slurry).

Live cell Ca²⁺ imaging—First, the cells were pre-incubated in a serum-free extracellular medium (ECM, 120 mM NaCl, 5 mM NaHCO₃, 10 mM Na-HEPES, 4.7 mM KCl, 1.2 mM KH₂PO₄, 1.2 mM MgSO₄, 2 mM CaCl₂, 10 mM glucose, pH7.4) containing 2% BSA. For SOCE experiments, ER stores were depleted by 10 min pretreatment with 2 μ M thapsigargin in Ca²⁺-free ECM. For permeabilized cells imaging, mitochondrial loading with 4 μ M Fura-FF AM was performed for 1h at 37°C, in in a serum-free extracellular medium (ECM, 120 mM NaCl, 5 mM NaHCO₃, 10 mM Na-HEPES, 4.7 mM KCl, 1.2 mM KH₂PO₄, 1.2 mM MgSO₄, 2 mM CaCl₂, 10 Mm glucose, pH7.4) containing 2% BSA and 0.012% Pluronic Acid. After plasma membrane permeabilization for 5 min at 37°C with 40 μ g/ml sap onin, cells were washed once with ICM and then incubated with ICM supplemented with 2 mM MgATP, 2 μ M thapsigargin, 2 mM Succinate, 20 μ M CGP-37157 and 1 μ M Rhod2-FA. Fluorescence wide field imaging of [Ca²⁺]_c and [Ca²⁺]_m was carried out using a ProEMICU1024 EM-CCD (Princeton Instruments), fitted to Leica DMI 6000B inverted epifluorescence microscopes as previously described (Paillard et al., 2017).

QUANTIFICATION AND STATISTICAL ANALYSIS

Data are expressed as mean \pm SEM. Experiments were performed at least 3 times, in duplicates or more. Statistical analysis was performed using ANOVA-1 followed by a Dunn's post-hoc test for comparisons between multiple groups.

Supplementary Material

Refer to Web version on PubMed Central for supplementary material.

ACKNOWLEDGEMENTS

MP was a recipient of postdoctoral fellowships from La Fondation pour la Recherche Médicale (FRM) and American Heart Association and a grant “Aide à la mobilité” from the Institut Servier (France). The study was funded by an NIH grant (RO1 GM102724) to GH.

REFERENCES

- Antony AN, Paillard M, Moffat C, Juskeviciute E, Correnti J, Bolon B, Rubin E, Csordas G, Seifert EL, Hoek JB, et al. (2016). MICU1 regulation of mitochondrial Ca(2+) uptake dictates survival and tissue regeneration. *Nat Commun* 7, 10955. [PubMed: 26956930]
- Arduino DM, Wettmarshausen J, Vais H, Navas-Navarro P, Cheng Y, Leimpek A, Ma Z, Delrio-Lorenzo A, Giordano A, Garcia-Perez C, et al. (2017). Systematic Identification of MCU Modulators by Orthogonal Interspecies Chemical Screening. *Molecular cell* 67, 711–723 e717. [PubMed: 28820965]
- Baughman JM, Perocchi F, Girgis HS, Plovanich M, Belcher-Timme CA, Sancak Y, Bao XR, Strittmatter L, Goldberger O, Bogorad RL, et al. (2011). Integrative genomics identifies MCU as an essential component of the mitochondrial calcium uniporter. *Nature* 476, 341–345. [PubMed: 21685886]
- Cao C, Wang S, Cui T, Su XC, and Chou JJ (2017). Ion and inhibitor binding of the double-ring ion selectivity filter of the mitochondrial calcium uniporter. *Proceedings of the National Academy of Sciences of the United States of America* 114, E2846–E2851. [PubMed: 28325874]
- Chakraborty PK, Mustafi SB, Xiong X, Dwivedi SKD, Nesin V, Saha S, Zhang M, Dhanasekaran D, Jayaraman M, Mannel R, et al. (2017). MICU1 drives glycolysis and chemoresistance in ovarian cancer. *Nature communications* 8, 14634.
- Csordas G, Golénar T, Seifert EL, Kamer KJ, Sancak Y, Perocchi F, Moffat C, Weaver D, de la Fuente Perez S, Bogorad R, et al. (2013). MICU1 controls both the threshold and cooperative activation of the mitochondrial Ca(2)(+) uniporter. *Cell metabolism* 17, 976–987. [PubMed: 23747253]
- D MA, and Perocchi F (2018). Pharmacological modulation of mitochondrial calcium homeostasis. *The Journal of physiology*.
- Gutscher M, Pauleau AL, Marty L, Brach T, Wabnitz GH, Samstag Y, Meyer AJ, and Dick TP (2008). Real-time imaging of the intracellular glutathione redox potential. *Nature methods* 5, 553–559. [PubMed: 18469822]
- Hoffman NE, Chandramoorthy HC, Shamugapriya S, Zhang X, Rajan S, Mallilankaraman K, Gandhirajan RK, Vagnozzi RJ, Ferrer LM, Sreekrishnanilayam K, et al. (2013). MICU1 motifs define mitochondrial calcium uniporter binding and activity. *Cell reports* 5, 1576–1588. [PubMed: 24332854]
- Ji L, Liu F, Jing Z, Huang Q, Zhao Y, Cao H, Li J, Yin C, Xing J, and Li F (2017). MICU1 Alleviates Diabetic Cardiomyopathy Through Mitochondrial Ca²⁺-Dependent Antioxidant Response. *Diabetes* 66, 1586–1600. [PubMed: 28292968]
- Kamer KJ, and Mootha VK (2014). MICU1 and MICU2 play nonredundant roles in the regulation of the mitochondrial calcium uniporter. *EMBO Rep* 15, 299–307. [PubMed: 24503055]
- Kovacs-Bogdan E, Sancak Y, Kamer KJ, Plovanich M, Jambhekar A, Huber RJ, Myre MA, Blower MD, and Mootha VK (2014). Reconstitution of the mitochondrial calcium uniporter in yeast. *Proceedings of the National Academy of Sciences of the United States of America* 111, 8985–8990. [PubMed: 24889638]
- Lewis-Smith D, Kamer KJ, Griffin H, Childs AM, Pysden K, Titov D, Duff J, Pyle A, Taylor RW, Yu-Wai-Man P, et al. (2016). Homozygous deletion in MICU1 presenting with fatigue and lethargy in childhood. *Neurol Genet* 2, e59. [PubMed: 27123478]
- Liu JC, Liu J, Holmstrom KM, Menazza S, Parks RJ, Fergusson MM, Yu ZX, Springer DA, Halsey C, Liu C, et al. (2016). MICU1 Serves as a Molecular Gatekeeper to Prevent In Vivo Mitochondrial Calcium Overload. *Cell reports* 16, 1561–1573. [PubMed: 27477272]
- Liu JC, Parks RJ, Liu J, Stares J, Rovira II, Murphy E, and Finkel T (2017). The In Vivo Biology of the Mitochondrial Calcium Uniporter. *Advances in experimental medicine and biology* 982, 49–63. [PubMed: 28551781]

- Logan CV, Szabadkai G, Sharpe JA, Parry DA, Torelli S, Childs AM, Kriek M, Phadke R, Johnson CA, Roberts NY, et al. (2014). Loss-of-function mutations in MICU1 cause a brain and muscle disorder linked to primary alterations in mitochondrial calcium signaling. *Nat Genet* 46, 188–193. [PubMed: 24336167]
- Mallilankaraman K, Doonan P, Cardenas C, Chandramoorthy HC, Muller M, Miller R, Hoffman NE, Gandhirajan RK, Molgo J, Birnbaum MJ, et al. (2012). MICU1 Is an Essential Gatekeeper for MCU-Mediated Mitochondrial Ca(2+) Uptake that Regulates Cell Survival. *Cell* 151, 630–644. [PubMed: 23101630]
- Mammucari C, Gherardi G, and Rizzuto R (2017). Structure, Activity Regulation, and Role of the Mitochondrial Calcium Uniporter in Health and Disease. *Frontiers in oncology* 7, 139. [PubMed: 28740830]
- Matlib MA, Zhou Z, Knight S, Ahmed S, Choi KM, Krause-Bauer J, Phillips R, Altschuld R, Katsube Y, Sperelakis N, et al. (1998). Oxygen-bridged dinuclear ruthenium amine complex specifically inhibits Ca²⁺ uptake into mitochondria in vitro and in situ in single cardiac myocytes. *The Journal of biological chemistry* 273, 10223–10231. [PubMed: 9553073]
- Oxenoid K, Dong Y, Cao C, Cui T, Sancak Y, Markhard AL, Grabarek Z, Kong L, Liu Z, Ouyang B, et al. (2016). Architecture of the mitochondrial calcium uniporter. *Nature* 533, 269–273. [PubMed: 27135929]
- Paillard M, Csordas G, Szanda G, Golenar T, Debattisti V, Bartok A, Wang N, Moffat C, Seifert EL, Spat A, et al. (2017). Tissue-Specific Mitochondrial Decoding of Cytoplasmic Ca²⁺ Signals Is Controlled by the Stoichiometry of MICU1/2 and MCU. *Cell reports* 18, 2291–2300. [PubMed: 28273446]
- Patron M, Checchetto V, Raffaello A, Teardo E, Vecellio Reane D, Mantoan M, Granatiero V, Szabo I, De Stefani D, and Rizzuto R (2014). MICU1 and MICU2 finely tune the mitochondrial Ca²⁺ uniporter by exerting opposite effects on MCU activity. *Molecular cell* 53, 726–737. [PubMed: 24560927]
- Petrungaro C, Zimmermann KM, Kuttner V, Fischer M, Dengjel J, Bogeski I, and Riemer J (2015). The Ca(2+)-Dependent Release of the Mia40-Induced MICU1-MICU2 Dimer from MCU Regulates Mitochondrial Ca(2+) Uptake. *Cell metabolism* 22, 721–733. [PubMed: 26387864]
- Plovanich M, Bogorad RL, Sancak Y, Kamer KJ, Strittmatter L, Li AA, Girgis HS, Kuchimanchi S, De Groot J, Speciner L, et al. (2013). MICU2, a paralog of MICU1, resides within the mitochondrial uniporter complex to regulate calcium handling. *PLoS One* 8, e55785. [PubMed: 23409044]
- Raffaello A, De Stefani D, Sabbadin D, Teardo E, Merli G, Picard A, Checchetto V, Moro S, Szabo I, and Rizzuto R (2013). The mitochondrial calcium uniporter is a multimer that can include a dominant-negative pore-forming subunit. *The EMBO journal*.
- Sancak Y, Markhard AL, Kitami T, Kovacs-Bogdan E, Kamer KJ, Udeshi ND, Carr SA, Chaudhuri D, Clapham DE, Li AA, et al. (2013). EMRE is an essential component of the mitochondrial calcium uniporter complex. *Science* 342, 1379–1382. [PubMed: 24231807]
- Tsai MF, Phillips CB, Ranaghan M, Tsai CW, Wu Y, Williams C, and Miller C (2016). Dual functions of a small regulatory subunit in the mitochondrial calcium uniporter complex. *Elife* 5.
- Vecellio Reane D, Vallese F, Checchetto V, Acquasaliente L, Butera G, De Filippis V, Szabo I, Zanotti G, Rizzuto R, and Raffaello A (2016). A MICU1 Splice Variant Confers High Sensitivity to the Mitochondrial Ca²⁺ Uptake Machinery of Skeletal Muscle. *Molecular cell* 64, 760–773. [PubMed: 27818145]
- Wang L, Yang X, Li S, Wang Z, Liu Y, Feng J, Zhu Y, and Shen Y (2014). Structural and mechanistic insights into MICU1 regulation of mitochondrial calcium uptake. *The EMBO journal* 33, 594–604. [PubMed: 24514027]
- Xue Q, Pei H, Liu Q, Zhao M, Sun J, Gao E, Ma X, and Tao L (2017). MICU1 protects against myocardial ischemia/reperfusion injury and its control by the importer receptor Tom70. *Cell Death Dis* 8, e2923. [PubMed: 28703803]

Highlights

- MICU1 controls the RuRed/Ru360 sensitivity of the MCU complex
- MICU1's R440/443 supports a direct interaction with MCU
- MICU1 R440/443-dependently competes with RuRed for interacting the D-ring of MCU
- MICU1-MCU interaction is central for MCU gatekeeping and cell survival

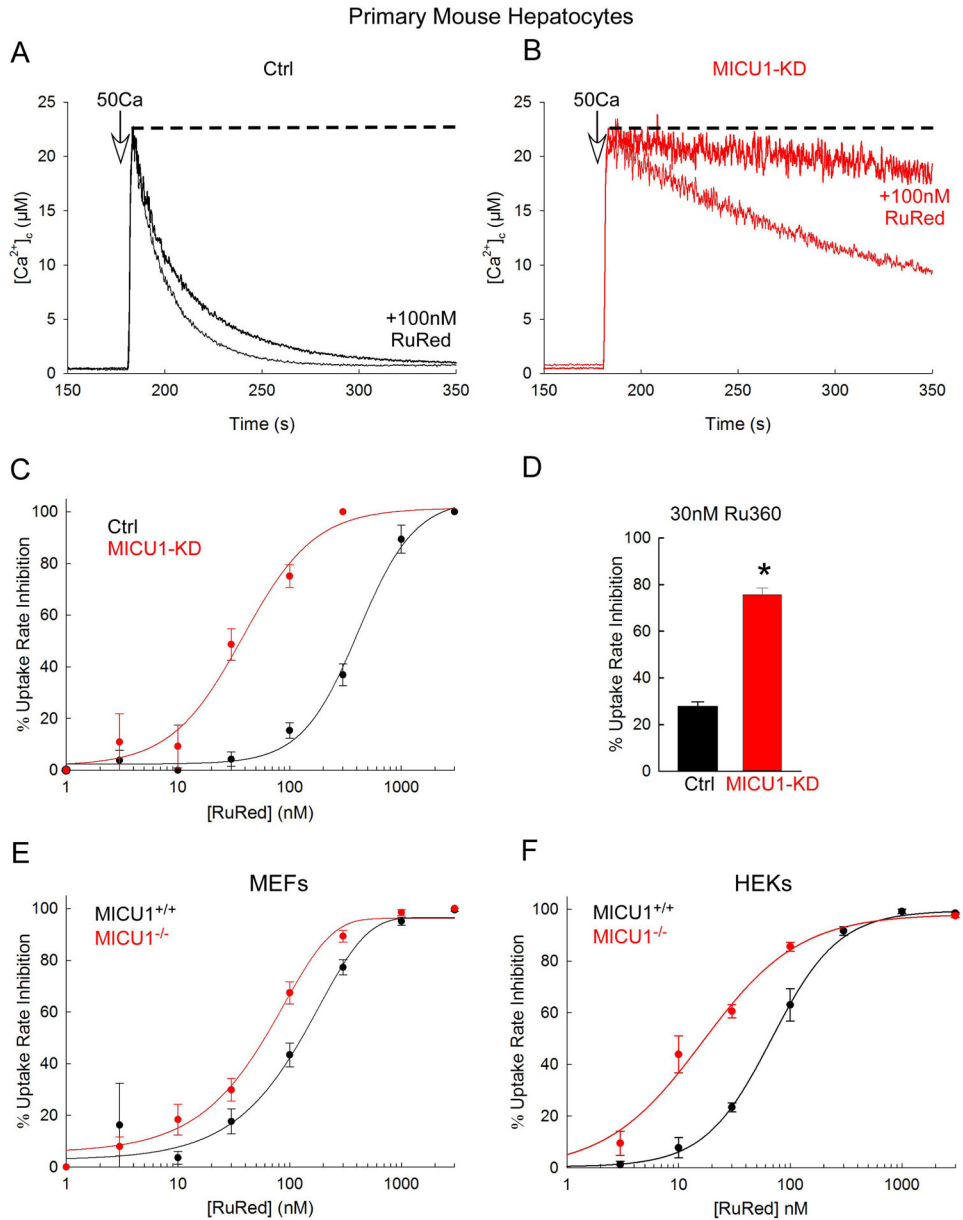


Figure 1: MICU1 controls the RuRedRu360 sensitivity of MCU complex

A-B) Time courses of the mitochondrial clearance of the $[Ca^{2+}]_i$ rise upon addition of a 50 μM $CaCl_2$ bolus (50Ca) in permeabilized Ctrl (A) and MICU1-KD hepatocytes (B), with and without 100nM RuRed. Dashed line indicates complete inhibition of the mitochondrial Ca^{2+} uptake.

C) [RuRed] dose response for the percentage of inhibition of the initial mitochondrial uptake rate for a 50Ca bolus in Ctrl (black) and MICU1-KD (red) hepatocytes. A sigmoidal fit is displayed for each.

D) Percentage of uptake rate inhibition by 30nM Ru360 in Ctrl (black) and MICU1-KD (red) hepatocytes.

E-F) [RuRed] dose response for the percentage of uptake rate inhibition for a 20Ca bolus in MICU1^{+/+} and MICU1^{-/-} MEFs (E) and HEKs (F). A sigmoidal fit is displayed for each.

Mean \pm SEM, n=3-4, * p<0.05 vs Ctrl, t-test.
See also Figure S1.

Author Manuscript

Author Manuscript

Author Manuscript

Author Manuscript

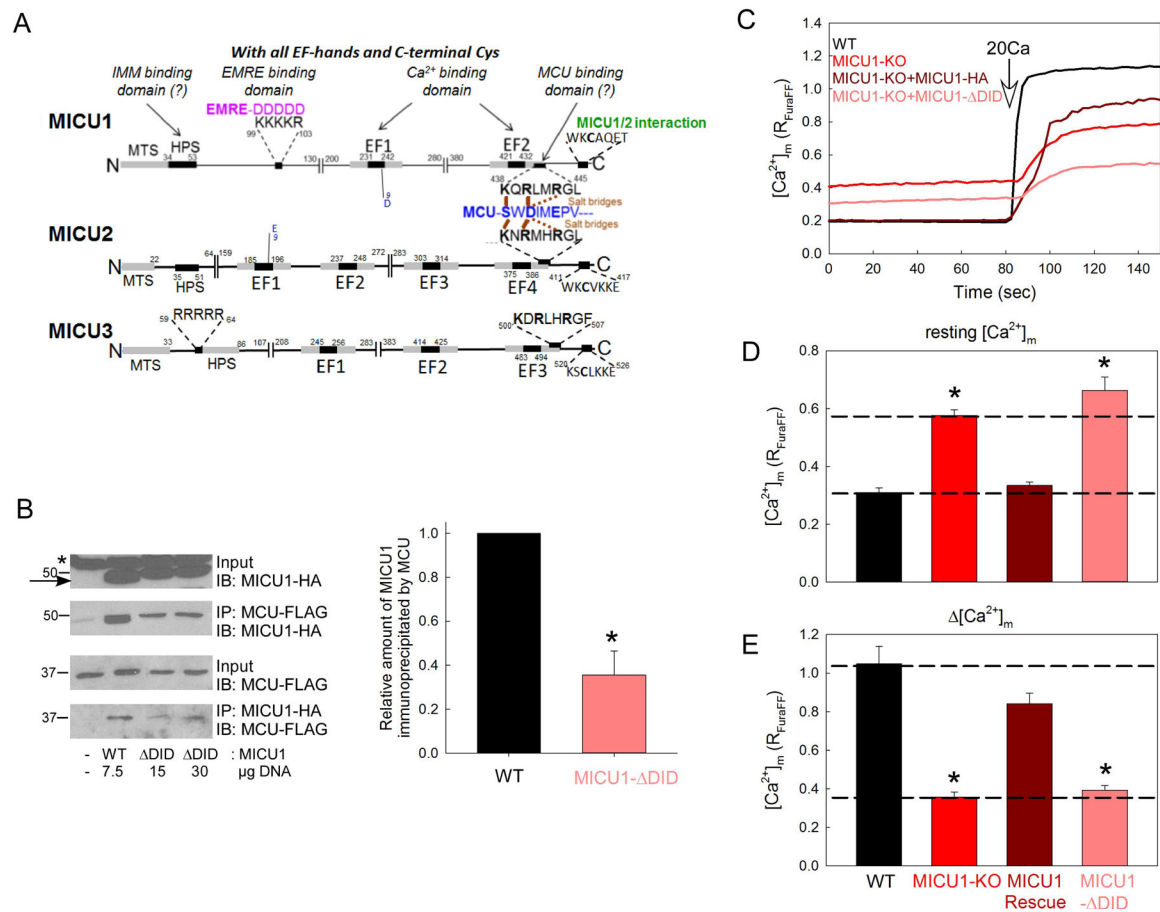


Figure 2: Mutation of the complementing sequence interferes with MICU1 binding to and control of MCU

A) Alignment of MICU1, 2 and 3 showing previously identified sites in MICU1 involved in interactions with EMRE and MICU1/2, and proposing a potential MCU binding domain.

B) Upper: Representative immunoblotting of co-IP between MCU-FLAG and HA-tagged WT MICU1 or MICU1- DID mutant expressed in MCU-FLAG HEKs. Arrow indicates specific MICU1-HA band while asterisk is an unspecific band. Lower: Quantification of the relative MICU1 amount pulled down by MCU-FLAG in HEK cells expressing WT MICU1 or MICU1- DID. Mean ± SEM, n=3, * p<0.05 vs WT, t-test.

C) [Ca²⁺]_m measurements in permeabilized WT MEFs and MICU1-KO MEFs expressing empty vector, MICU1 or MICU1- DID and challenged with a bolus of 20μM CaCl₂.

D) Quantification of resting [Ca²⁺]_m as an index of thresholding of the MCU complex.

E) Calculations of the difference (Δ[Ca²⁺]_m) between the [Ca²⁺]_m 30s post-20Ca addition and the resting [Ca²⁺]_m as an index of cooperativity of the MCU complex.

Mean ± SEM, n=6, * p<0.05 vs WT, one-way ANOVA.

See also Figure S2.

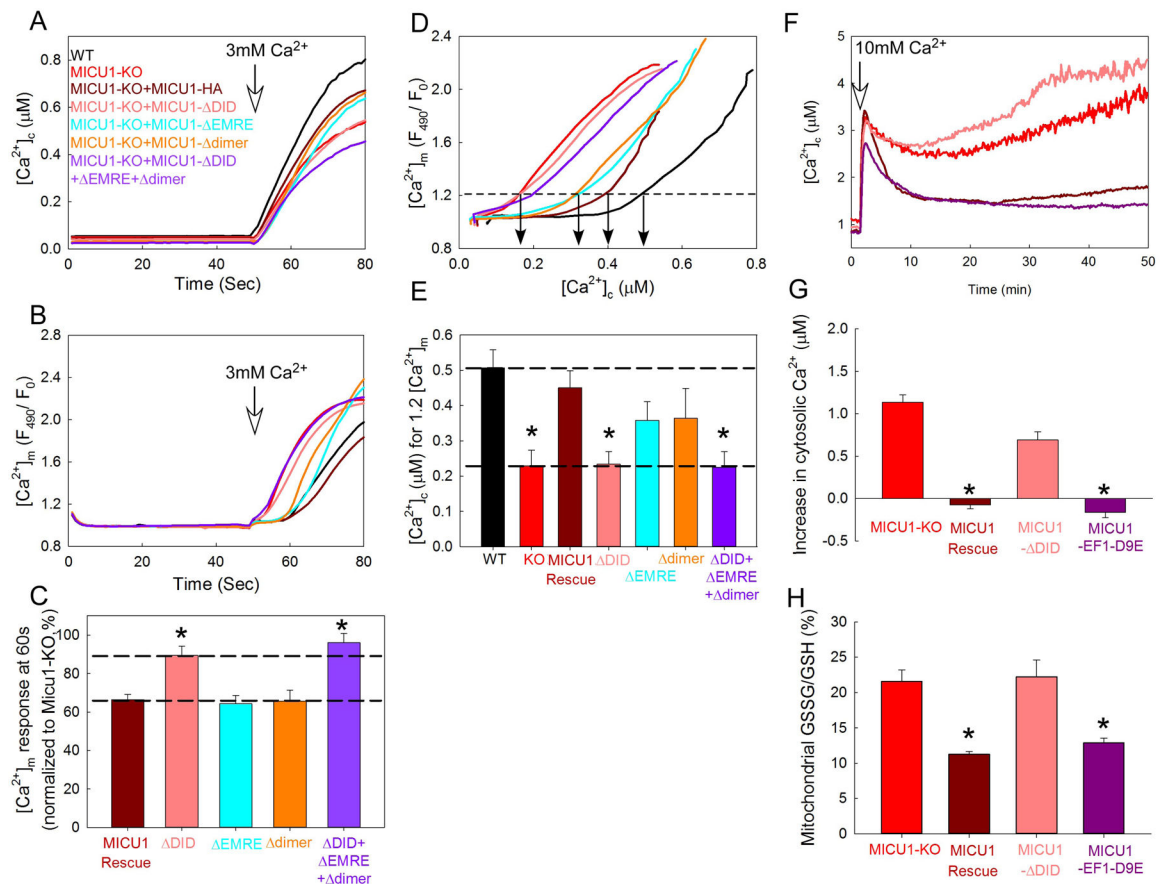


Figure 3: Critical role of the DID of MICU1 in Ca²⁺ homeostasis and cell survival.

A-B) SOCE-induced [Ca²⁺]_c (A: Fura2 after calibration in μM) and [Ca²⁺]_m (B: mt-Cepia) time courses in WT and MICU1-KO HEKs expressing the indicated MICU1 constructs, after addition of 3mM CaCl₂.

C) Bar graph shows [Ca²⁺]_m response at 60s, normalized to MICU1-KO HEKs response, from data in (B).

D) [Ca²⁺]_m plotted against [Ca²⁺]_c in individual cells.

E) Measurements of [Ca²⁺]_c required to reach 1.2 [Ca²⁺]_m on data from (D). Mean ± SEM, n=4-7, * p<0.05 vs WT, one-way ANOVA.

F) Representative traces of [Ca²⁺]_c measured by fura-ff-AM in intact HEKs cells after an addition of 10mM CaCl₂ and in presence of 100μM H₂O₂.

G) Quantification of the increase in [Ca²⁺]_c from data in (F) (50min-10min).

H) Quantification of the mitochondrial GSSG/GSH ratio using the mtGrx1-RoGFP2 sensor in the same conditions as in (F).

Mean ± SEM, n=3 independent experiments, * p<0.05 vs MICU1-KO, one-way ANOVA.

See also Figure S3 and S4.

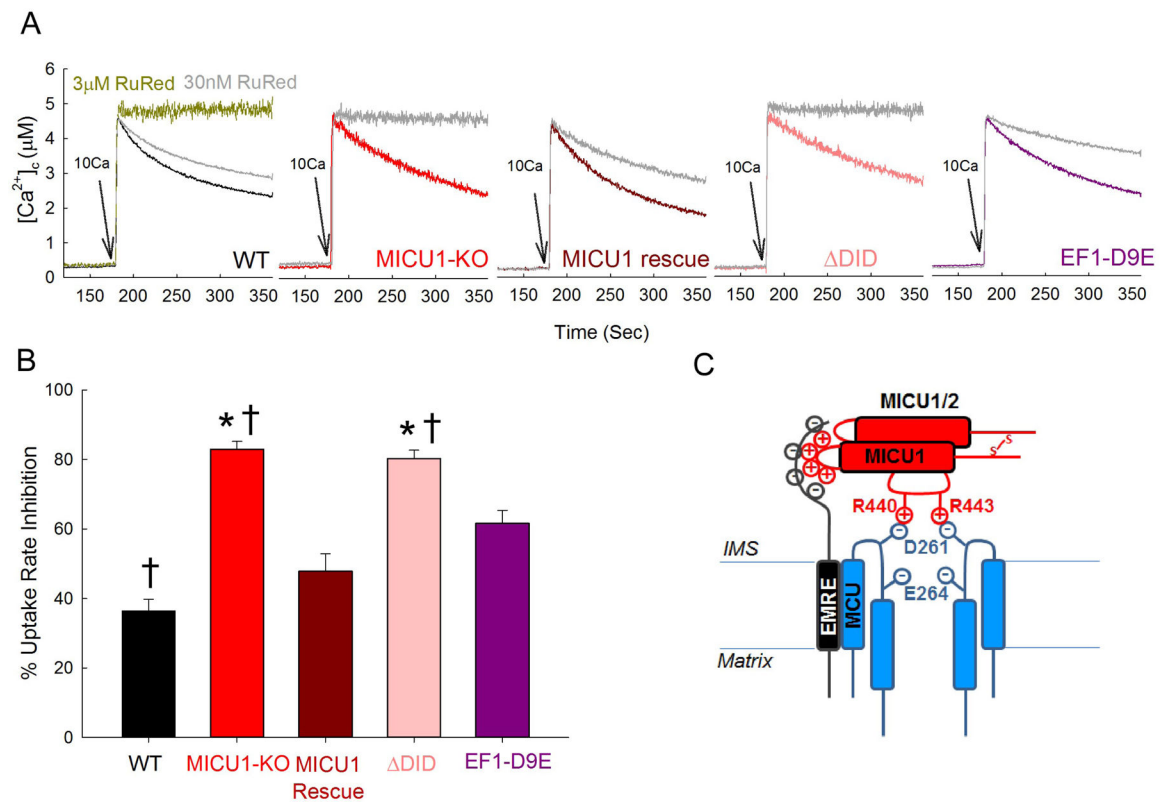


Figure 4: MICU1-MCU interaction through the DID of MICU1 is required to maintain RuRed sensitivity.

A) Time courses of the mitochondrial clearance of the [Ca²⁺]_c rise upon addition of a 10 μ M CaCl₂ bolus (10Ca) in permeabilized WT and MICU1-KO HEKs with different MICU1 constructs, with or without RuRed (3 μ M or 30nM).).

B) Bar graph shows percentage of uptake rate inhibition by 30nM RuRed in data from (A). Mean \pm SEM, n=3, * p<0.05 vs WT, † p<0.05 vs MICU1-EF1-D9E, one-way ANOVA.).

C) Proposed model for MICU1 interaction with the MCU complex. In addition to the previously identified sites of MICU1 interaction with MICU1/2 through a disulfide bridge and with EMRE via electrostatic binding, we have identified a new functional domain in MICU1, the DID, for interaction with the DIME domain of MCU. More precisely, the two arginines 440 and 443 in MICU1 would interact via salt bridges with the accessible D-ring of the filter selectivity domain of MCU, to control the Ca²⁺ flux and RuRed sensitivity of the MCU complex.).

See also Figure S4.

KEY RESOURCES TABLE

REAGENT or RESOURCE	SOURCE	IDENTIFIER
Antibodies		
Rabbit anti-MICU1	Sigma-Aldrich	HPA037480
Rabbit anti-MCU	Sigma-Aldrich	HPA016480
Rabbit anti-MICU2	Abcam	ab101465
Mouse anti-mtHsp70	Thermo Fisher	MA3-028
Rabbit anti-prohibitin	Abcam	ab28172
Anti-HA polyclonal	Invitrogen	71-5500
Anti-FLAG M2	Sigma-Aldrich	F1804
Anti-Myc monoclonal	Precision	AG10004
Chemicals, Peptides, and Recombinant Proteins		
Anti-DYKDDDDK (FLAG) beads	Genscript	A00187-200
Ruthenium Red	Sigma	R2751
Fura-2 (AM)	Teflabs	0-103
Fura-2 (salt)	Teflabs	0-104
Fura-2 low affinity (AM)	Teflabs	0-136
Fura-2 low affinity (salt)	Teflabs	0-137
Thapsigargin	Enzo Life Sciences	BML-PE180-0005
CGP-37157	Enzo Life Sciences	BML-CM119-0005
Lipofectamine 3000	Life Technologies	L3000008
Complete protease inhibitor cocktail (EDTA free)	Roche	11873580001
Protein A Sepharose	Abcam	ab193256
Critical Commercial Assays		
DC Protein Assay	Biorad	5000112
Experimental Models: Cell Lines		
MICU1 ^{loxP/loxP} MEF	Antony et al., 2016	N/A
MICU1 ^{KO/KO} MEF	Antony et al., 2016	N/A
MICU1-KO HEK293T	Sancak et al., 2013	N/A
EMRE-KO HEK293T	Sancak et al., 2013	N/A
HEK293T stably overexpressing mouse MCU-FLAG	O-Uchi et al., 2014	N/A
WT HEK293T	Sancak et al., 2013	N/A
Recombinant DNA		
pcDNA-dest40-MICU1-HA	Kamer et al., 2017	N/A
pcDNA3.1-MICU1-C465A-HA	Patron et al., 2014	N/A
pcDNA-dest40-M1-EF1-D9E-HA, M1- DID-HA and M1- EMRE-HA	This paper	N/A
EMRE-Myc	This paper	N/A
Mt-Cepia	This paper	N/A
mtGrx1-RoGFP	This paper	N/A
Software and Algorithms		
Canvas X	N/A	N/A

REAGENT or RESOURCE	SOURCE	IDENTIFIER
Endnote	N/A	N/A
SigmaPlot 12.5	N/A	N/A

Author Manuscript

Author Manuscript

Author Manuscript

Author Manuscript